Effect of Pre-strain on the Solute Clustering, Mechanical Properties, and Work-Hardening of a Naturally Aged Al-Cu-Mg Alloy

D. SHAO, P. ZHANG, J.Y. ZHANG, G. LIU, R.H. WANG, W.Q. LIU, G. SHA, and J. SUN

The effect of pre-strain on the solute clustering, mechanical properties, and work-hardening of a naturally aged Al-Cu-Mg alloy was comprehensively investigated using a three-dimensional atom probe, electrical resistivity, and hardness measurements. The pre-strain promoted the rapid formation of solute clusters but suppressed the growth of solute clusters during prolonged aging. An increase in pre-strain caused a decrease in the saturated number density of solute clusters, leading to a reduction in cluster strengthening. By taking into account the coupling effect of solute clusters and pre-existing dislocations, models were proposed to address the yield strength and work-hardening behaviors of the Al-Cu-Mg alloy, respectively. It reveals that the solute-cluster strengthening is comparable to dislocation strengthening in the naturally aged alloy. However, the work hardening is not significantly affected by the presence of the solute clusters. The findings reported in this paper will be helpful for the development of a naturally aged Al-Cu-Mg alloy with improved performance by controlling the pre-strain.

I. INTRODUCTION

SOLUTE clustering and precipitation are key processes responsible for strengthening aluminum alloys. A comprehensive understanding of these processes is necessary for a better control of aging treatments and optimization of the mechanical properties of the Al alloys. While the precipitation has been extensively studied using transmission electron microscopy (TEM),[1–3] characterization of the solute clustering is more challenging and requires high-resolution characterization tools to resolve these ultrafine solute clusters.[4,5] A three-dimensional atom probe (3DAP) is a powerful tool for revealing the three-dimensional distribution of individual atoms in materials. It has recently been used in studying the growth kinetics,[6–8] composition,[8–10] and number density[11,12] of solute clusters in the Al alloys. The nuclear magnetic resonance (NMR) technique has been used in quantifying the fractions of solute atoms in solid solutions and in the clusters.[13–15] In addition, the positron annihilation lifetime spectroscopy (PALS) technique is capable of providing information about vacancy behavior during clustering.[16–18] All these techniques help to understand solute clustering and reveal the influence of the solute clustering on mechanical properties of the Al alloys.

Solute clusters are characteristic microstructural features of naturally aged (NA) aluminum alloys, such as NA Al-Mg-Si alloys[16,19] and Al-Cu-Mg alloys.[20,21] The solute clusters formed before artificial aging or at the early stage of artificial aging will remarkably affect the subsequent age-hardening response of some alloys in either a beneficial[22] or a detrimental[23] manner. Some models have been proposed[7,24–26] to quantitatively describe solute clustering and its interaction with dislocations, which help to understand the correlation between the macroscopic properties and atomic-level structures.

The quick formation of solute clusters has long been correlated with the accelerated diffusion of solute atoms due to the presence of excess quenched-in vacancies.[27,28] Advanced experimental examinations shed more light in elucidating the solute clustering process. For example, PALS measurements[29,30] have demonstrated that some solutes (e.g., Sn and Ag) are capable of stabilizing the quenched-in vacancies in Al for an

D. SHAO, P. ZHANG, J.Y. ZHANG, G. LIU, and J. SUN are with the State Key Laboratory for Mechanical Behavior of Materials, Xi'an Jiaotong University, Xi'an, 710049, China. Contact e-mails: lgsammer@mail.xjtu.edu.cn; junsun@mail.xjtu.edu.cn R.H. WANG is with the School of Materials Science and Engineering, Xi'an University of Technology, Xi'an 710048, China. W.Q. LIU is with the Key Laboratory for Microstructure, Shanghai University, Shanghai 200444, China. G. SHA is with the School of Materials Science and Engineering, Nanjing University of Science and Technology, Nanjing 210094, China. Contact e-mail: gang.sha@njust.edu.cn

extended period of time, over which the solute clustering occurs. A combined examination of 3DAP and electrical resistivity has suggested that each vacancy contributes to the formation of up to ten clusters, and each vacancy transports in excess of 1000 solute atoms to clusters in an Al-Mg-Si-Cu alloy.[31]

The recognition of the key role of vacancies in solute-cluster formation led to the first quantitative model addressing the clustering process in Al alloys, which was proposed by Girifalco and Herman.[27] The model, referred to as the vacancy jump model, was based on the idea that vacancy-solute complexes form and diffuse down a concentration gradient to the growing cluster.[27] Although the modeling results are reasonably consistent with the resistivity testing results of some Al alloys, some assumptions made in this model are questionable. In particular, it is assumed that the binding between a vacancy and single solute atoms is strong, but that between a vacancy and a solute cluster is weak. This assumption is irreconcilable with the common understanding. To overcome this problem, Zurob and Seyedrezai[24] recently proposed another model based on the idea that vacancies spend most of their time by trapping in clusters. In this model, the escape of vacancies was presented as the rate-limiting process for cluster growth, and the number of solute atoms in clusters was predicted to increase linearly with the logarithm of time.[24] This modeling prediction was consistent with their electrical resistivity results. In addition to these analytical models, other attempts based on a phase-field crystal model[32,33] and Monte Carlo simulations[34] have been made, with the aim of determining the mechanisms of formation and growth of solute clusters at the atomic scale. Phase-field crystal modeling[32] revealed that the formation of early subcritical clusters was triggered by the stress relaxation effect of quenched-in defects on the energy barrier and the critical size for nucleation.

Solute-cluster strengthening, which is termed cluster hardening, was originally proposed to interpret the early rapid age-hardening effect of Al-Cu-Mg alloys.[35,36] Areal glide simulations suggest that the spatial distribution of weak obstacles (e.g., the solute-solute clusters) minimally affects the alloy strength.[37] This implies that the strengthening response of solute clusters observed experimentally should be associated with chemical and/or elastic effects. An analytical model for cluster strengthening due to the short-range order has been proposed for solute dimers in Al-Cu-Mg and Al-Mg-Si alloys.[26,38] These previous theoretical investigations are only limited to considering solute dimmers or larger clusters, but no elastic effect has been considered. Recently, by considering the cluster elastic effect, Zhao[25] proposed a size misfit strengthening model, which should be adequate for handling small solute clusters with sizes less than 1 nm in diameter in the NA Al alloys.

To date, there is a lack of research comprehensively addressing solute-cluster growth and strengthening in the Al alloys containing dislocations. Such research is important for better understanding strengthening effect of Al alloys reinforced with second phase particles, such as SiC-particle-reinforced AA2009 alloy (Al-Cu-Mg-based alloy), which has been used as extruded tubes for helicopters.[39] The alloy is usually subjected to natural aging treatment (termed T4), and forms solute clusters in the Al matrix. During material preparation, the presence of the second phase particles will inevitably cause internal stress/strain and induce geometrically enabled dislocations to accommodate the thermal expansion mismatch between the matrix and the reinforcement particles.[40,41] In this research area, there are following fundamental questions remaining to be addressed: (i) the effects of stress/strain and dislocations on solute clustering, (ii) the interplay between solute clusters and dislocations in strengthening and work-hardening, and (iii) the relationship between the solute clusters and the mechanical properties.

In this paper, an Al-Cu-Mg alloy under different levels of pre-strain (PS) will be naturally aged, and the effect of PS and pre-existing dislocations on solute clustering, mechanical properties, and deformation behaviors will be investigated comprehensively. The choice of the Al-Cu-Mg alloy as the studied material is based on following considerations: (i) Al-Cu-Mg alloys are classic Al alloys used in studying solute clustering and cluster hardening[7,25,38]; and (ii) the Al-Cu-Mg alloy comprises the base of an industrially important T4-treated 2009 Al alloy reinforced with SiC particles. PS will be applied to mimic the internal strain which affects solute clustering during natural aging. Both experimental and modeling work conducted by research aims to correlate solute clusters with mechanical properties of the alloy.

II. EXPERIMENTAL PROCEDURES

A. Material Preparation and Heat Treatments

An Al-Cu-Mg alloy with a nominal composition of Al-3.6 wt pct Cu-1.6 wt pct Mg was prepared by powder metallurgy. The alloy powders (with an average diameter of 30 μm) were milled for 7 hours with a milling intensity of 160 rpm. Consolidation was performed by uniaxial hot pressing at 823 K and finally hot extruding at 723 K with a ratio of 15:1 by using a 2000 KN hydraulic press machine. This resulted in consolidated bulk cylinders with a relative density of about 99.9 pct measured by using the Archimedes principle. The extruded bars produced from the consolidated cylinders have a diameter of 10 mm. They were solutionized at 773 K for 1 hour, quenched in water at ambient temperature, compressed with different plastic reductions of 0, 2.0, 4.5, 6.0, and 9.0 pct, and naturally aged for different periods of time (up to 96 hours). Note that the compression was performed promptly after quenching, applied along the extrusion direction, and unloaded once the targeted deformation was reached. All compressions were completed within approximately 20 minutes, and the timing of natural aging began after each sample was quenched into the water. The maximum error of all temperature measurements in the present experiments was ±0.1 K. Figure 1(a) illustrates the process of heat treatment and pre-straining.
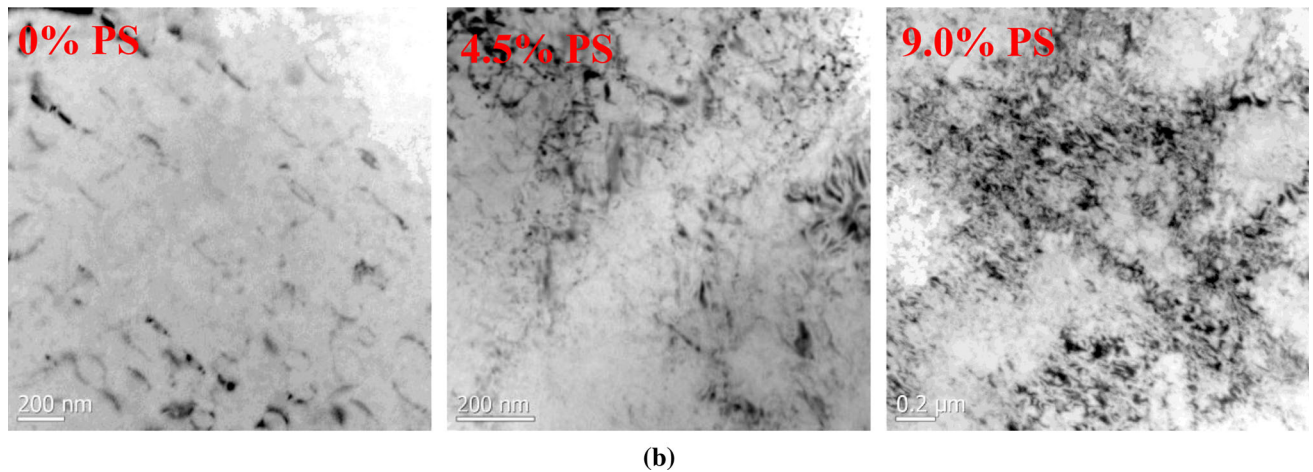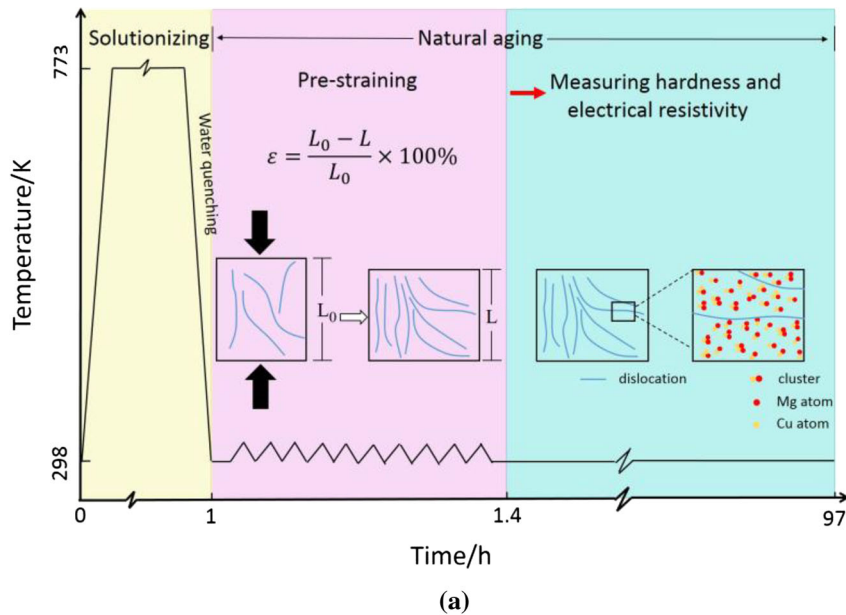
Fig. 1—(a) A schematic diagram illustrating the heat treatments, pre-straining, and involved microstructural evolution. (b) TEM images of the Al-Cu-Mg alloy with PS = 0 pct, PS = 4.5 pct and 9.0 pct to show the dislocations.

B. Microstructural Characterizations

The microstructures and textures of the NA Al-Cu-Mg alloy were characterized by electron backscattered diffraction (EBSD), which was performed on a high-resolution JSM 7001F fitted with a Pegasus XM2-EBSD system operating at 20 kV. Specimens for EBSD observations were prepared by electro-polishing using an electrolyte consisting of 25 pct nitric acid and 75 pct methanol at 253 K (–20 °C) for 1 minute at an operation voltage of 15 V. The EBSD analyses were conducted on the planes parallel and perpendicular to the extrusion direction, respectively. The texture measurement results are presented in the form of orientation distribution functions (ODF) in the sections with φ_2 being a constant.

Pre-existing dislocations in the alloy after NA treatment were examined with a transmission electron microscope (TEM) which was performed on a JEOL-2100 microscope operating at 200 kV. The TEM foils were prepared following the standard electro-polishing techniques for Al alloys.[42,43] The dislocation density in each specimen was determined using a line-intercept method.[44] At least 200 grains were measured to obtain the statistical data. X-ray Diffraction (XRD) peak broadening, as an alternative approach, was used to measure the microstrain and dislocation density, based on the Williamson–Hall method.[45–47] XRD experiments were performed with a Rigaku D/max-RB X-ray diffractometer equipped with a Cu target and a graphite monochromator, at 40 kV, 40 mA and a scan speed of 0.2 deg minute^{-1}.

Three-dimensional atom probe (3DAP) experiments were performed using a CAMECA local electrode atom probe (LEAP 4000HR). APT sample blanks with a square cross-sectional area of approximately 0.3 × 0.3 mm^2 and a length of 10 mm were prepared by a combination of slicing and mechanical grinding. A two-step electropolishing procedure was used to produce 3DAP sharp tips from these blanks.[43] A solution of 10 vol pct perchloric acid in methanol was used for

coarse polishing, and the final polishing was performed using a solution of 2 vol pct perchloric acid in butoxyethanol. 3DAP data collection was performed under voltage pulsing at a specimen temperature of 30 ± 0.3 K with a voltage pulse fraction (pulse voltage/steady-state DC voltage) of 20 pct, a pulse repetition rate of 200 kHz under a vacuum $<6.7 \times 10^{-8}$ Pa (5×10^{-10} torr).

Quantitative determination of the number density of clusters (per cubic cm) was performed on the experimental data by using the maximum separation method as described in Reference 48. A nearest-neighbor (NN) analysis was performed to monitor differences between the experimental and random-labeled cumulative NN distance histograms.[7]

C. Measurements of Electrical Resistivity and Mechanical Properties

The electrical resistivity of each specimen aged at different time was measured at 77 K in liquid nitrogen using a custom-made four-point probe system. The resistance (R) was used to calculate the resistivity (ρ) with the equation $\rho = RA/L$, where A is the cross-sectional area of the sample, and L is the distance between the two potential probes. To minimize the testing error, we used $\Delta\rho/\rho_0 = (R - R_0)/R_0$ to represent the relative change in electrical resistivity, where ρ_0 is electrical resistivity of the as-compressed sample, and R and R_0 are the resistance values of the samples after and before NA, respectively.

Hardness measurements were performed on a LECO Hardness Tester (LV700AT) under a weight of 5 kg and with a dwelling time of 10 seconds. Uniaxial tensile testing was used to determine yield strength (σ_0) and measure the work hardening. But the testing was only applied to the alloy naturally aged to 96 hours, because the alloy has the relatively stable solute clusters (see the Section III–B). Tensile specimens have a reduced section of 6 mm in width and 50 mm in length, with axis along the extrusion direction. The testing was performed at a constant strain rate of 5×10^{-4} s^{-1} with the load direction parallel to the specimen axis. The yield strength was determined as the 0.2 pct offset.

III. RESULTS

A. Dislocations, Grains, and Texture of the Naturally Aged Alloy

TEM examinations, as shown in Figure 1(b), revealed that dislocations were highly present in the alloy with no PS. They were likely introduced by the powder metallurgy processing. The number density of the dislocations notably increased with the applied PS. The dislocation densities, measured from both TEM examinations and XRD analyses, are listed in Table I. The two sets of results measured by using the two techniques were in broad agreement with each other. The number density of dislocations in the alloy with a PS of 9.0 pct was found to be over an order of magnitude greater than

that in the strain-free alloy. In the following section, the dislocation density derived from TEM measurements will be used for modeling.

Figures 2(a), (b), (e), and (f) display representative EBSD images to show the grains on the planes perpendicular (a and e) and parallel (b and f) to the extrusion direction of the samples with a PS of 0 pct (a and b) and 9.0 pct (e and f), respectively. The average grain size is ~150 μm in both 0 and 9.0 pct PS samples, which indicates that the application of PS up to 9.0 pct has no effect on the grain size. Figures 2(c), (d), (g), and (h) show the corresponding texture analyses along the extrusion direction of the samples with a PS of 0 pct (c and d) and 9.0 pct (g and h) in the $\varphi_2 = 45$ deg (c and g) and $\varphi_2 = 90$ deg (d and h) sections, respectively. The texture of the samples consists of a mixture of brass (B), cube, S and β-fiber texture components. The texture information calculated by ODF is given in Table II.

B. Evolution of Electrical Resistivity and Hardness with Aging Time

Because the natural aging occurred at room temperature, the annihilation of strain-induced dislocations was ignored in this research. The relative change in resistivity and hardness during aging was used to elucidate the dislocation effect and the clustering effect of the alloy. The evolution of $\Delta\rho/\rho_0$ with aging time (t) is plotted in Figure 3(a). Two regimes are discernible in the plots of the samples at different PSs. The regime I corresponds to aging time (t) less than approximately 27 hours, where $\Delta\rho/\rho_0$ increases linearly with the logarithm of t. The regime II corresponds to aging time (t) greater than 27 hours, where $\Delta\rho/\rho_0$ reaches a plateau and is insensitive to t. The critical point of t (~27 hours) is independent of the PS, but the slope of the $\Delta\rho/\rho_0$ vs $ln(t)$ curve decreases with increasing in the PS.

To confirm the above observation, we examined the hardness measurements. Figure 3(b) shows the evolution of hardness with $ln(t)$ of the samples with different PSs. Since the number density of dislocations was weakly changed as the function of aging time, the increment in hardness was mainly correlated to the hardening from the time-dependent solute clustering. The strain-free alloy displayed the highest increment, which was due to the most active formation of solute clusters. This observation is consistent with that previously observed from the electrical resistivity measurements. In contrast, the hardness of the 9.0 pct pre-strained alloy did not show any significant change during the entire aging process, indicating that straining-hardening became predominant under the high strain.

C. Solute Clusters from the 3DAP Analyses

The effect of PS on solute clusters was analyzed using 3DAP, and the examined samples were aged for 96 hours within the regime II reaching to a saturation condition in the resistivity of the alloy samples. Figures 4(a) through (c) shows the reconstructed three-dimensional atom maps of Cu and Mg in the 96

Table I. Statistical Results on the Parameters of Microstructural Features of the Al-Cu-Mg Alloy with Different PS

Pre-Strain	Dislocation Density (10^{13}/m^2)		Concentrations of Solute Atoms in Solid Solution (pct)		Parameters of the Cu-Mg Solute Clusters		
	TEM	XRD	Cu	Mg	Average Size (atoms)	Average Guinier Radius (nm)	Volume Fraction (vol pct)
0 pct	0.50 ± 0.05	0.51 ± 0.10	1.397 ± 0.03	1.384 ± 0.02	6.54 ± 0.1	0.415 ± 0.005	0.381 ± 0.04
2.0 pct	3.81 ± 0.23	2.54 ± 0.63	1.398 ± 0.04	1.387 ± 0.07	6.50 ± 0.1	0.413 ± 0.002	0.377 ± 0.03
4.5 pct	9.02 ± 1.04	7.92 ± 1.24	1.404 ± 0.02	1.393 ± 0.04	6.48 ± 0.1	0.410 ± 0.003	0.372 ± 0.02
6.0 pct	18.54 ± 1.22	15.24 ± 3.25	1.410 ± 0.05	1.396 ± 0.03	6.45 ± 0.1	0.408 ± 0.005	0.365 ± 0.03
9.0 pct	40.34 ± 5.53	28.45 ± 4.13	1.412 ± 0.02	1.399 ± 0.05	6.43 ± 0.2	0.406 ± 0.004	0.361 ± 0.02

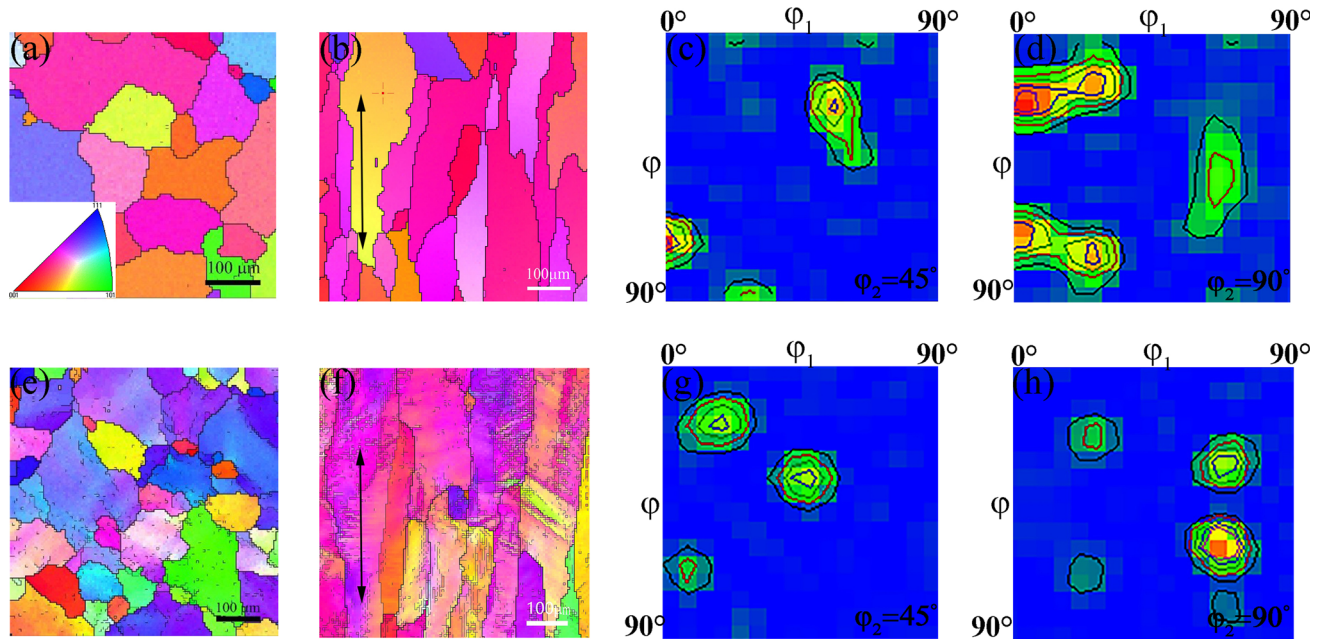All the samples for 3DAP examinations are naturally aged to 96 h.

Fig. 2—Representative EBSD results of the Al-Cu-Mg alloy with PS = 0 pct (*a* and *b*) and 9.0 pct (*e* and *f*) on the plane perpendicular to and along extrusion direction to show the grain size and morphology. The arrows in (b) and (f) indicate the extrusion direction. The texture evolution along the extrusion direction is presented in the form of orientation distribution functions (ODF) in the φ_2 = 45 deg and φ_2 = 90 deg sections with PS = 0 pct (*c* and *d*) and 9.0 pct (*g* and *h*).

Table II. EBSD Results on the Textures of the Al-Cu-Mg Alloy with Different PS

Pre-Strain	Texture Components (pct)				Taylor Factor ($M \varphi$ = 0 deg, ϕ = 0 deg)
	Brass (B)	Cube	S	β-Fiber	
0 pct	9.27	2.92	5.72	3.21	3.08
4.5 pct	15.82	1.44	6.06	2.96	3.09
9.0 pct	22.31	0.45	6.11	2.51	3.11

hours-aged alloy samples with PS values of 0, 4.5, and 9.0 pct, respectively. No microstructural features in these total atom maps could be clearly observed by simple visual examinations. Careful nearest-neighbor (NN) analysis using the IVAS computer software can easily resolve a very small change of solute distribution in these analyzed volumes by detecting any deviation of the atom distribution of a certain alloy element between an experimental atom probe data and a reference dataset with atoms in the random distribution.[7,11] This

technique is extremely useful for revealing solute element behaviors during the very early stage of decomposition of materials.

Figures 5(a) and (b) show the NN analysis results of Mg and Cu, respectively, in 96 hours-aged alloy samples with PS values of 0 and 9.0 pct. In both PS-free and highly pre-deformed alloy samples, the NN distance histogram of Mg atoms in the experimental dataset distinctly deviated from the reference NN distance histogram of the corresponding random datasets. This
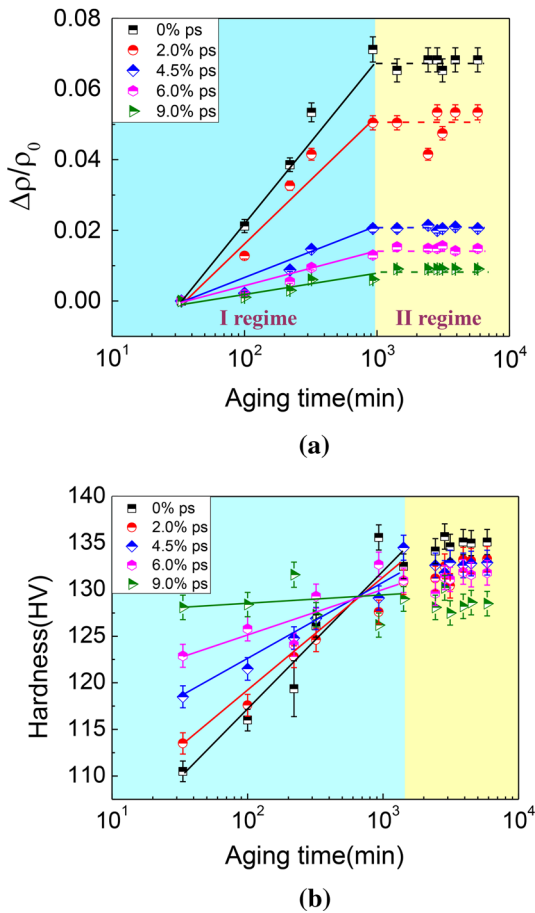
(a)

(b)

Fig. 3—Variation of the relative change in electrical resistivity ($\Delta\rho/\rho_0$) (*a*) and the hardness (*H*) (*b*) with aging time in the Al-Cu-Mg alloy with different PSs.

indicated that Mg atoms in the alloy samples developed a non-random distribution, regardless of the application of PS or not. The non-random distribution of Mg atoms in the alloy was attributed to the formation of solute clusters.

Using the maximum separation method,[48] solute clusters were identified in the analyzed volumes (see Figures 5(c) and (d) for the samples with PS = 0 and 9.0 pct, respectively). The displayed volumes for Figures 5(c) and (d) are the same in size, each is a subset taken from the entirely analyzed dataset. Hence, the difference of the clusters within the displayed volumes was obvious. The solute clusters were statistically countered. Figure 6(a) shows the number density of solute clusters of the alloy with 0, 4.5, and 9.0 pct PS, where the clusters are sorted into different groups according to their sizes. This figure reveals that very few solute clusters have a size of more than ten solute atoms. Approximately, 90 pct of the solute clusters contains less than six solute atoms. This is due to that the activation energy for cluster growth is relatively low in natural aging. Similar phenomenon has been observed in naturally aged Al-Mg-Si-based alloys.[7] In contrast, solute clusters with larger sizes (*e.g.*, greater than 20 atoms) were frequently found in artificially aged Al alloys.[7,11] Here, solute clusters with two atoms

include (i) binary clusters containing unlike solute atoms, *i.e.*, Cu-Mg, and (ii) binary clusters containing like solute atoms, *i.e.*, Cu-Cu and Mg-Mg. The fractions of each type solute clusters (*i.e.*, the Cu-Mg, Cu-Cu, and Mg-Mg clusters) over the total binary clusters are shown in Figure 6(b). It is likely that Cu atoms may predominantly segregate to the dislocations. As a result, Cu-Cu clusters with a higher concentration were detected in the sample with a 9.0 pct reduction (Figure 6(b)).This explanation is consistent with the segregation behavior of alloying elements observed in AA2024 alloys.[9] Another important finding from Figure 6(a) is that the number density of solute clusters decreased with increasing in PS. This is consistent with the electrical resistivity and hardness measurements presented previously. PS seems to suppress the formation of solute clusters. The statistical results of the Cu-Mg solute clusters are summarized in Table I and will be used to model the cluster contributions to hardness and work-hardening values in the following sections.

IV. DISCUSSION

Our experimental results demonstrated that PS had important influence on the solute clustering, mechanical properties, and deformation behaviors of the NA Al-Cu-Mg alloy. The resistivity and 3DAP results indicated that further solute clustering was suppressed in the samples with the presence of high-density dislocations due to a high PS applied (over 4.5 pct reduction) after rapid initial clustering. This suggestion is consistent with that the resistivity increase of the alloy during natural aging becomes smaller with increasing in the PS. The strength of the alloy was found to increase with increasing PS. In this section, the effect of PS on solute clustering will first be clarified in terms of thermodynamic/kinetic analyses. Subsequently, the contributions of solute clusters to strength and deformation behaviors will be quantitatively described by developing strengthening and work-hardening models, respectively.

A. *Effect of Pre-strain on Solute Clustering*

Electrical resistivity measurements have been proven to be sensitive for detecting solute clustering in Al alloys.[31,49,50] During natural aging or the initial stages of precipitation, the resistivity of the Al alloys increases as solute clusters form and grow, even though this process leads to the removal of solute atoms from the solid solution. To understand this phenomenon, one must consider the effects of both solute atoms and solute clusters on resistivity. The effect of solute atoms on the overall resistivity is usually described by Matthiessen's Law.[51] However, the examination of the contribution of resistivity from solute clusters is more complex. It is generally believed that the strong electrons scattering induced by solute clusters causes an increase in the resistivity. The resistivity contribution from solute clusters is hence dependent on both the size and number density of the solute clusters. The following equation
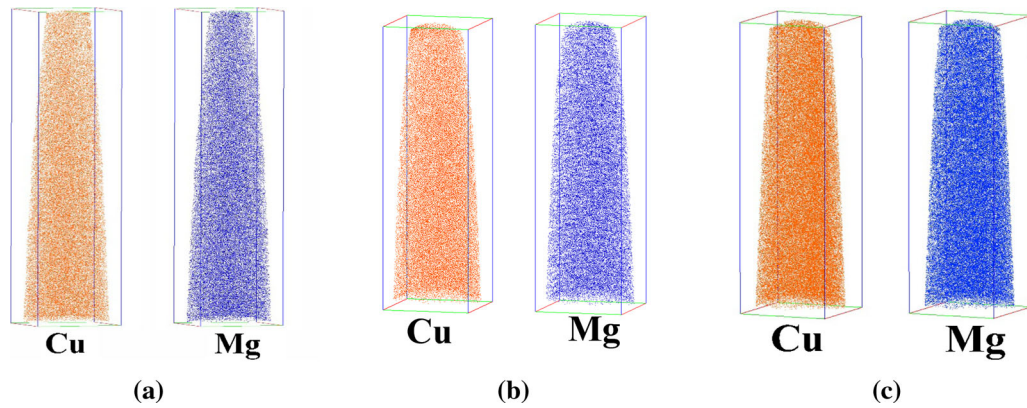
Fig. 4—Atom maps of Cu and Mg in the 96 h-naturally aged Al-Cu-Mg alloy samples with PS 0 (*a*), 4.5 pct (*b*), and 9.0 pct (*c*).

has been suggested[28] to quantify the relative increase in resistivity, $\Delta\rho/\rho_0$, related to the formation of solute clusters:

$$\Delta\rho/\rho_0 = \sum N_i \rho_i + N \cdot f(n), \qquad [1]$$

where N_i is the number of i solute atoms in solution (i = Cu or Mg for the present alloy), ρ_i is the resistivity contribution per solute atom, N is the number of solute clusters, n is the size (number of solute atoms) of each cluster, and $f(n)$ represents cluster resistivity as a function of the cluster size. Previous work has assumed that $f(n) \propto n^{0.8}$[28] or $f(n) \propto n$.[27] For simplicity, the latter form ($f(n) \propto n$) is use here. Because N_i is equal to $(N_{i0} - N \cdot n)$, where N_{i0} is the total number of solute atoms, i, in the alloy, the above equation can be rewritten as

$$\Delta\rho/\rho_0 = k_1 + k_2 \cdot N \cdot n, \qquad [2]$$

where k_1 and k_2 are constants. By assuming that N is constant, Zurob and Seyedrezai[24] found that $\Delta\rho/\rho_0$ changes linearly with n. They further proposed[24] a simple cluster growth model to correlate n with aging time (t). This model is based on the postulation that the attractive interaction between solutes and vacancies results in the trapping of vacancies at clusters. Provided that the escape of vacancies from existing clusters is the rate-limiting step for cluster growth, n is predicted to be proportional to the logarithm of aging time (t). Finally, $\Delta\rho/\rho_0 \propto \ln(t)$ is derived,[24] which is consistent with some electrical resistivity results.[31,49,50]

In the present work, our 3DAP results, as shown in Figure 6(a), clearly demonstrated that (i) approximately 90 pct of the solute clusters were small in size and contained less than ten solute atoms after a natural aging of 96 hours; and (ii) the applied PS has slightly effect on the cluster size while greatly affected the cluster number density in the alloy aged for 96 hours. Similar experimental observations have been made by other research in different Al alloys.[31,52] For example, using 3DAP examinations, Aruga et al.[51] evaluated continuous changes in the number density, size, and chemical composition of Mg-Si clusters in an Al-Mg-Si alloy during natural aging, and found that the average size

and chemical composition were nearly unchanged, but the number density was notably increased. Ferragut et al.[52] observed an increase in the electrical resistivity in an Al-Zn-Cu-Mg alloy aged near room temperature, and they ascribed the resistivity change to the volume fraction growth of pre-precipitate solute clusters according to their detailed analyses. Therefore, it is reasonable to assume that solute clustering in the NA Al-Cu-Mg alloy is predominantly controlled by increasing in the number density of the solute clusters rather than the growth of their size. In other words, n changes slightly with t, while N changes notably with t. By considering the size of solute clusters (n) as a constant, N should be approximately scaled with $\ln t$, as deduced from Eq. [2] by using quantitative data showing in Figure 6(a). The experimental results of $\Delta\rho/\rho_0$ vs the logarithm of aging time (t) show a relationship (see Figure 3(a)). This is similar to the prediction by Zurob and Seyedrezai's model,[24] although the basic assumptions made in Zurob and Seyedrezai's model is greatly in contrast with that used in our model.

The vast dislocations induced by the PS improved the diffusion of alloying elements, and hence initially accelerated the formation of solute clusters because the solute atoms were readily shifted by dislocations and then aligned along the dislocations.[53] On the other hand, the dislocations are preferential sinks for vacancies, which will result in vacancy annihilation and drastically reduce the vacancy concentration in the matrix with increasing aging time.[54] Because vacancies play an important role in the formation of solute clusters,[24,27] solute clustering in the matrix away from dislocations will be suppressed in the case of a reduced vacancy concentration. The two factors were predominant at different stages of aging, and they were responsible for the observed clustering behaviors in the alloy under different PSs. In the alloy with a PS = 9.0 pct, dislocations were plentiful, and therefore rapid formation of solute clusters was highly favored. A large number of solute clusters were promptly formed within a short time. The number density of solute clusters would become nearly saturated at the initial aging stage (before the resistivity and hardness measurements) and only slightly changed during the following aging stages. This is the reason why both the measured resistivity and
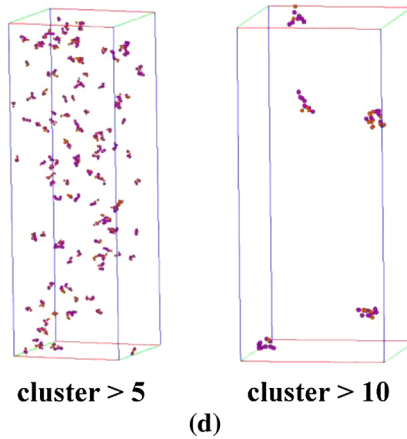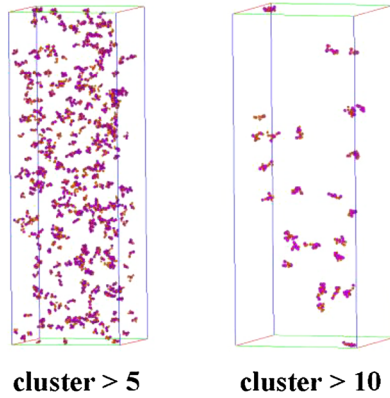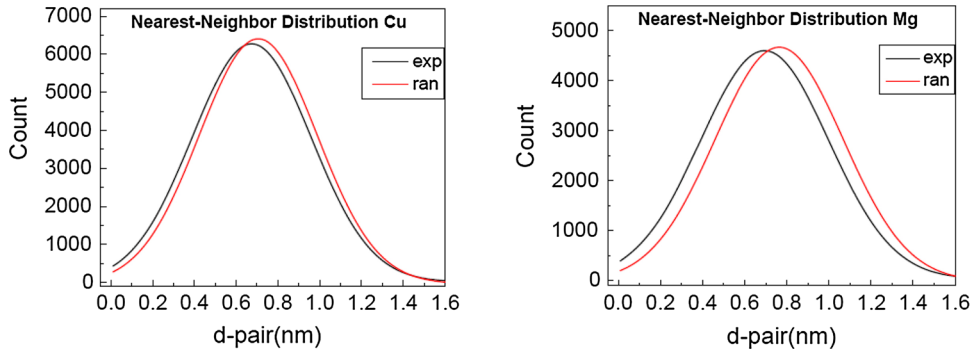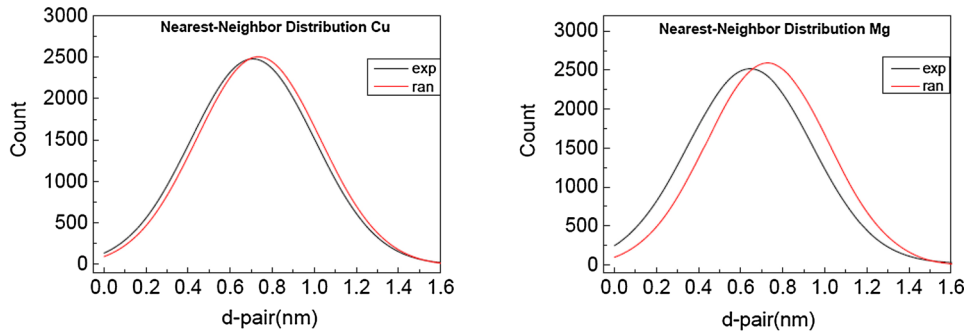
Fig. 5—NN analysis results of Mg and Cu in the Al-Cu-Mg alloy samples with PS of 0 (*a*) and 9.0 pct (*b*). Combined atom maps show only solute clusters containing more than 5 and 10 solute atoms in the Al-Cu-Mg alloy with PS of 0 (*c*) and 9.0 pct (*d*). All volumes are 20 × 20 × 60 nm.
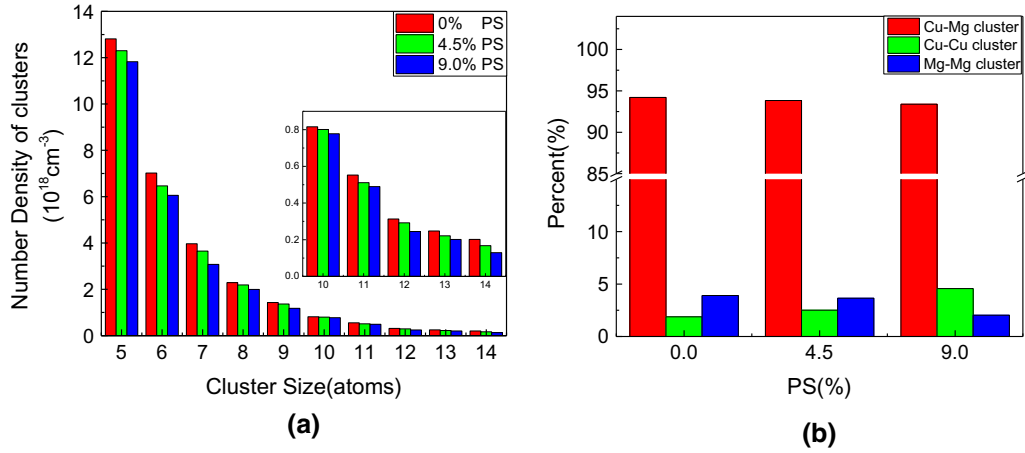
Fig. 6—(*a*) Statistical results of the number density of solute clusters in the Al-Cu-Mg alloy with PS values of 0, 4.5, and 9.0 pct, where the clusters are sorted into different sizes. The insert shows a magnified portion of a cluster with a size greater than six atoms. (*b*) The fractions of the Cu-Mg, Cu-Cu, and Mg-Mg clusters of the binary clusters in the Al-Cu-Mg alloy with PS values of 0, 4.5, and 9.0 pct.

hardness hardly changed with aging time (see Figure 3). At the opposite extreme, few dislocations were present in the PS-free alloy, and the cluster formation kinetics should be slow without the dislocations-assisting diffusion. The number density of the solute clusters would be gradually increased with increasing aging time, and it finally reached saturation after more than 27 hours. When a greater PS was applied, a stronger acceleration effect would occur and more clusters were formed in the initial aging stage. In summary, PS accelerated solute clustering (a promoting effect) during short-term aging, but suppressed the further formation of new solute clusters during prolonged aging, and caused a reduction in the final number density of the solute clusters (a degrading effect) at the maximum hardness.

B. *Strengthening of Solute Clusters*

Figure 3(b) reveals the combined effect of solute clusters and strain (dislocations) on strengthening the NA Al-Cu-Mg alloy under different PSs. In order to investigate the importance of solute-cluster strengthening, we used a theoretical approach to carefully evaluate the contributions of major strengthening mechanisms operated in the alloy, based on our experimental data. In this section, we will first evaluate the effect of PS on texture and concomitantly on Taylor factor. Subsequently, we will apply strengthening models to calculate the yield strength of the alloy with different PSs, in comparison with the experimental results. Both the yield strength before (without solute clusters) and after naturally aging (with solute clusters) will be modeled, from which the strengthening contributions from solute clusters and dislocations can be separately derived. In order to avoid the formation of solute clusters during tensile sample preparation, the yield strength before naturally aging is obtained from the experimentally measured hardness of the samples immediately after the PS applied, *i.e.*, yield strength $\approx 3.0 \times$ hardness.[55] As to the 96-hour naturally aged samples that have stable solute clusters, the experimental yield strength is
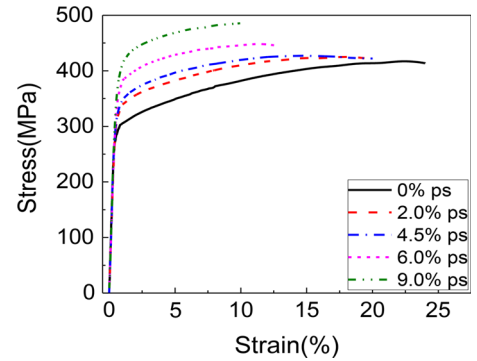

Fig. 7—Stress–strain curves of the 96 h-naturally aged Al-Cu-Mg alloy with different PSs.

measured from the tensile testing, see Figure 7 the stress-strain curves.

The yield strength of a polycrystalline material is known to be sensitive to the Taylor factor (M) that reflects the effects of alloy texture and the orientation of the tensile axis. The orientation angle φ is the angle between tensile axis and projection on to L-T plane, and ϕ is the angle between extrusion direction and projection on to L-T plane. Some models have been proposed to determine $M(\varphi, \phi)$,[56,57] and in this paper we employ the Taylor model to calculate M. For texture-free FCC metals, the Taylor model predicts $M_T = 3.07$.[58] But for the FCC metals with texture structure, the average M is given by Reference 59:

$$M(\varphi, \phi) = \sum_i \frac{f_i j_{max}}{\sum_{j=1}^{j_{max}} m_{ij}}, \qquad [3]$$

where i stands for each grain, m_{ij} is the values of the Schmid factor for the 12 directions of the {111}⟨110⟩ slip systems in the FCC structure. The Schmid factors are ordered such that $m_{i1} > m_{i2} > m_{i3}$, *etc.* f_i is the volume fraction of grains, j represents the activated slip systems

($j_{max} = 5$ for the Taylor model). In our experiments, the M ($\varphi = 0$ deg, $\phi = 0$ deg) (M in the extrusion direction) is considered. Based on the EBSD results, the value of M ($\varphi = 0$ deg, $\phi = 0$ deg) can be calculated by using Eq. [3], as shown in Table II for the 0 pct PS and 9.0 pct PS samples. The M ($\varphi = 0$ deg, $\phi = 0$ deg) of 9.0 pct PS sample is only ~1.0 pct higher than the 0 pct PS sample, indicative of small effect of PS on the M.

The yield strength (σ_y) of the NA Al-Cu-Mg alloy mainly include the dislocation strengthening (σ_d), grain boundary strengthening (σ_{gb}), solid solution strengthening (σ_{ss}), and solute cluster strengthening ($\sigma_{cluster}$). These strengthening components are considered to be additive in determining the yield strength of an alloy,[7] and can be written as

$$\sigma_y = \sigma_0 + \sigma_d + \sigma_{gb} + \sigma_s = \sigma_0 + \sigma_d + \sigma_{gb} + \left(\sigma_{ss}^q + \sigma_{cluster}^q\right)^{1/q},$$
[4]

where σ_0 is the base strength arising from friction stress, σ_s is the contribution to strength from both non-clustered solute atoms and solute clusters, and q is the addition law exponent with a value between 1.0 and 2.0.[60] The dislocation strengthening is related to the dislocation density (ρ_d)

$$\sigma_d = M \alpha G b \sqrt{\rho_d},$$
[5]

where M is the Taylor factor (~3.1[61]), α is a constant with a value of approximately 0.24,[62] G and b are the shear modulus (28 GPa[42]) and Burgers vector (0.286 nm[42]) of Al.

The grain boundary strengthening is proportional to $d^{-1/2}$ (d: grain size) by following the Hall–Petch relationship[62]:

$$\sigma_{gb} = k_{HP} d^{-1/2},$$
[6]

where k_{HP} is the Hall–Petch constant of about 0.062 MPa/m$^{-1/2}$[63] The strength increment due to the solid solution depends on the concentrations (C_i) of Cu and Mg that are measured from the atom probe results. The individual contributions of the single Cu and Mg atoms are obtained by Reference 64:

$$\sigma_{ss}^i = \frac{0.9 MGb}{L_{ss}^i} \cos^{3/2}\left(\frac{\varphi_{ss}^i}{2}\right)\left(1 - \frac{\cos^5\left(\varphi_{ss}^i/2\right)}{6}\right), \quad [7-1]$$

$$L_{ss}^i = 3^{1/4} \cdot b/2 \cdot \sqrt{C_i} \quad (i = \text{Cu, Mg}), \qquad [7-2]$$

where φ_{ss}^i is the dislocation breaking angle for shearing of i solute atoms (178 deg for Cu and 177 deg for Mg[7]), and L_{ss}^i is the equivalent square spacing of i solute atoms. σ_{ss} is then given by Reference 61:

$$\sigma_{ss} = \sqrt{\sum_i \left(\sigma_{ss}^i\right)^2}, (i = Cu, Mg). \qquad [8]$$

For the alloy before naturally aging and without solute clusters, Eq. [4] is reduced to:

$$\sigma_y^s = \sigma_0 + \sigma_d + \sigma_{ss} + \sigma_{gb}. \qquad [9]$$

Using the microstructural parameters measured in present experiments, the yield strength of the alloy before naturally aging can be predicted by using above equation. The predictions are plotted in Figure 8(a) to compare with the experimental measurements, from which a good agreement is evident.

We next to estimate the strength contribution from the solute clusters ($\sigma_{cluster}$). Estimation of the strength contribution from solute clusters is a complex problem. Starink et al.[26] proposed a solute cluster strengthening model in which the order strengthening, modulus strengthening, and chemical strengthening were considered for shearable solute clusters. In particular, this model was devoted to co-cluster dimers or clusters containing unlike solute atoms. Zhao[25] considered the elastic effect of clusters and proposed a size misfit strengthening model, in which the size misfit of clusters was assumed to be the sum of elementary atomic misfits. This model, although applicable to clusters ≤~1 nm in diameter as in present work, does not apply to Cu-Mg clusters because the formation of Cu-Mg clusters is energetically favored, and hence the Cu-Mg clusters have a smaller elastic misfit than even single atoms.[25] Marceau et al.[7] estimated cluster strengthening using an areal glide model in which the dislocation-cluster interaction strength was assumed to be related to the cluster size on the glide plane. Here, the areal glide model is employed to quantitatively describe cluster strengthening because the cluster parameters obtained from 3DAP examinations can be readily incorporated into this model.

Marceau et al.[6] investigated the evolution of solute clusters during the early stages of elevated temperature aging of rapid hardening Al-Cu-Mg alloys. They showed that Cu-Mg clusters exhibited the most potent strengthening response, while the strength contributions from Cu-Cu and Mg-Mg clusters were less significant. According to their results, we consider the strengthening effect of only Cu-Mg clusters, which is given by the areal slide model as[7]:

$$\sigma_{cluster}^{Cu-Mg} = \frac{1.8 MT}{b \cdot L_{cluster}^{Cu-Mg}} \cos^{3/2}\left(\frac{\varphi_{cluster}^{Cu-Mg}}{2}\right)\left(1 - \frac{\cos^5\left(\varphi_{cluster}^{Cu-Mg}/2\right)}{6}\right),$$
[10-1]

$$L_{cluster}^{Cu-Mg} = \bar{r}_{Cu-Mg} \cdot \left(2 \cdot \pi/3 \cdot f_{Cu-Mg}\right)^{1/2}, \qquad [10-2]$$

where $\bar{r}_{Cu-Mg}$ and f_{Cu-Mg} are the average 3-D Guinier radius and volume fraction of the Cu-Mg clusters, respectively, which are determined from the analysis of the 3DAP data; $L_{cluster}^{Cu-Mg}$ is the average spacing of Cu-Mg clusters on the glide plane; $\varphi_{cluster}^{Cu-Mg}$ is the dislocation breaking angle for shearing of the Cu-Mg solute clusters; and T is the line tension, which is equal to $0.5 Gb^2$.[7] Finally, the strength contribution is predicted by

$$\sigma_s = \left[\sigma_{ss}^q + \left(\sigma_{cluster}^{Cu-Mg}\right)^q\right]^{1/q}(1.0 \leq q \leq 2.0). \qquad [11]$$

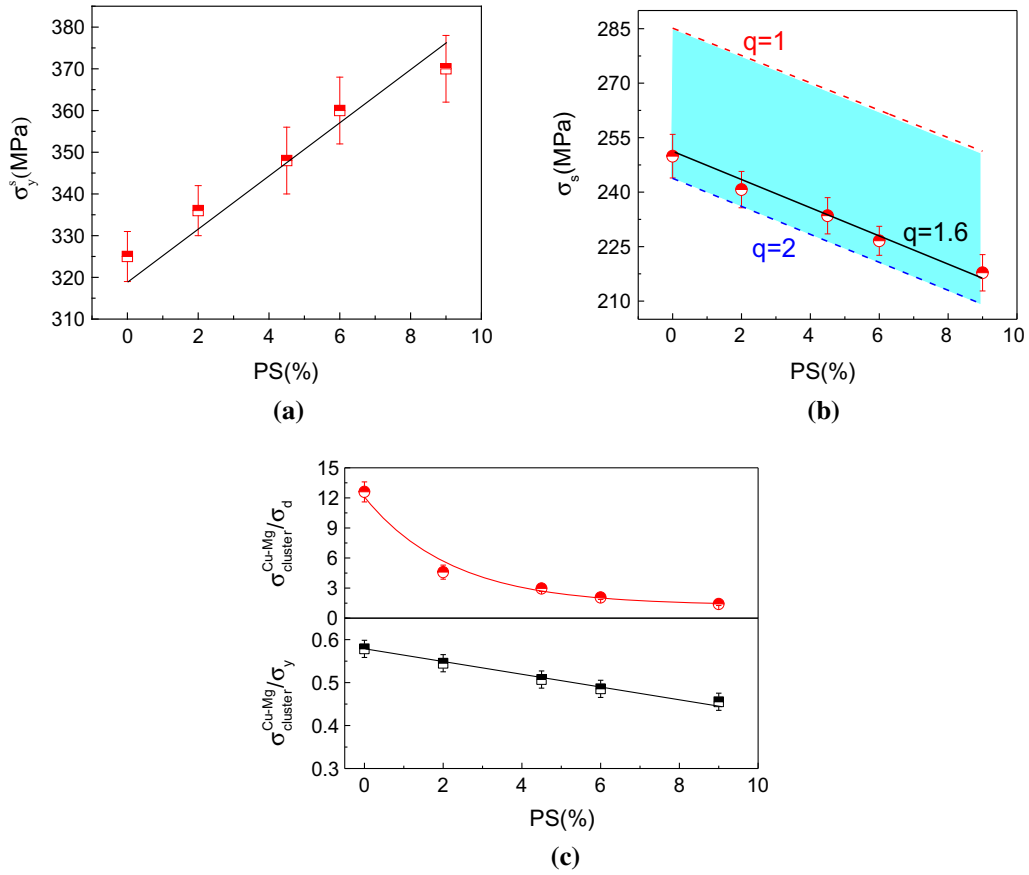Fig. 8—(a) Plot of σ_y^s vs PS. The dots represent experimental data and the line represents calculations. (b) Plots of σ_s vs PS. The dots represent experimental data and the lines represent calculations with $q = 1.0$ (uppermost dashed line), 1.3 (solid line), and 2.0 (bottommost dashed line). The shaded region represents a range of $1.0 \leq q \leq 2.0$. (c) Plots of $\sigma_{cluster}^{Cu-Mg}/\sigma_d$ and $\sigma_{cluster}^{Cu-Mg}/\sigma_y$ vs PS.

Hence, by rearranging Eq. [4], σ_s can be calculated by Eq. [12], with the experimental measurements of σ_y, σ_d calculated from Eq. [5] using ρ_d list in Table I and σ_{gb} calculated from Eq. [6] using grain size d measured by EBSD.

$$\sigma_s = \sigma_y - \sigma_0 - \sigma_d - \sigma_{gb}. \qquad [12]$$

The determined σ_s is plotted in Figure 8(b) as a function of the PS. This observation is consistent with the decrease in solute-clusters number density with increasing in PS, as found in Figure 6(a), and solute cluster strengthening appears to be much stronger than solution strengthening in the alloy. The calculations of the two limits, i.e., $q = 1.0$ and 2.0, are plotted in Figure 8(b) and compared with the experimental results. The experimental data fall into the predicted range between the two limits, and a calculation of $q = 1.6$ coincides with the experimental data, which is indicative of a good fit of the areal glide model to the present NA Al-Cu-Mg alloy. The relative contribution of Cu-Mg solute clusters is shown in Figure 8(c), where the ratios of $\sigma_{cluster}^{Cu-Mg}$ to σ_y and to σ_d are plotted as a function of the PS. The analysis results clearly demonstrated that the solute-clusters hardening, in comparison with dislocations hardening, is significant in determining to the hardness of the NA Al-Cu-Mg alloy.

C. Contribution of Solute Clusters to Work Hardening

The study of work hardening in metals, particularly the capability of the flow stress of the material to increase with increasing plastic strain, has attracted attention since the discovery of dislocations (see Reference 65 for a review) and is still a matter of wide current interest in the material with the presence of precipitates and solute clusters. The effect of unshearable precipitates on the work hardening of Al alloys has recently been quantitatively studied.[66,67] However, the effect of shearable solute clusters on work hardening remains unclear. Here, we will evaluate the contribution of solute clusters to the work hardening of the NA Al-Cu-Mg alloy.

In the Kocks–Mecking–Estrin model,[65] the athermal storage of moving dislocations is determined by the average spacing between the dislocations (i.e., $\rho_t^{-1/2}$). The evolution equation is as follows:

$$\frac{d\rho_t}{d\gamma} = K_1 \rho_t^{1/2} - K_2 \rho_t, \qquad [13]$$

where the mean density of forest dislocations (ρ_t) is a state variable. The first term describes the increase in the dislocation generation rate due to the increase in obstacle density caused by dislocation storage. The second term describes the change in dislocation density

due to dislocation annihilation. Coefficients K_1 and K_2 are parameters of the model, which characterize the rates of dislocation storage and dislocation annihilation, respectively. If the dislocation storage term dominates, the dislocation density increases according to γ^2. The evolution equation is further modified to include a mean free path for dislocation movement (l_t), which provides the following equation for dislocation generation[68]:

$$\frac{d\rho_t}{d\gamma} = (bl_t)^{-1} - K_2\rho_t. \qquad [14]$$

If the mean free path term dominates and is approximately constant, a critically resolved shear stress increment will be produced in proportion to the square root of the strain:

$$\Delta\tau = \alpha_1 Gb\sqrt{\rho_t} = \alpha_1 G\sqrt{b \cdot \gamma/l_t}. \qquad [15]$$

Considering that the Taylor factor in polycrystal metals and that the average plastic strain (ε_p) is related to the shear strain (γ) by $\varepsilon_p = M\gamma$, the strength increment is finally given by:

$$\Delta\sigma = \alpha_1 G\sqrt{Mb \cdot \varepsilon_p/l_t} = K_A\sqrt{\varepsilon_p}, \qquad [16]$$

where K_A is an alloy-dependent constant. This strength increase scaling with the square root of plastic strain (or a parabolic stress–strain curve) has been observed in a range of plastically non-homogeneous metal materials.[69] This proportionality is only valid over a limited strain range, which is alloy-dependent and has been estimated to be between ~0.01 and ~0.05.[69] In the Al alloys, the parabolic stress-strain curve has been related to the unshearable precipitates,[66,67] which are the direct micromechanical cause of the mean free path for dislocation movement. In the present work, similar parabolic stress-strain curves are found for the NA Al-Cu-Mg alloy that are characterized by shearable

solute clusters and pre-existing dislocations. To understand the deformation behavior in terms of the characteristic microstructures, we next evaluate the contributions of solute clusters and pre-existing dislocations to work hardening.

In the present case, the effective mean free path (l_t) includes portions related to the pre-existing dislocations (l_d) and to the solute clusters. Because the Cu-Mg clusters exhibit much stronger interactions with dislocations than the Cu-Cu and Mg-Mg clusters as mentioned above, only the Cu-Mg clusters are considered in the prediction of K_A. The mean free path of dislocations due to the Cu-Mg clusters is defined as l_{Cu-Mg} ($\propto N_{Cu-Mg}^{-1/3}$, N_{Cu-Mg}: number density of the Cu-Mg clusters). The superposition rule for l_d and l_{Cu-Mg} is $l_t^{-2} = l_d^{-2} + l_{Cu-Mg}^{-2}$.[68] In Starink et al.'s model,[70] K_A can be expressed as:

$$K_A = C_2 GM^{1/2}b^{1/2}\left(l_d^{-2} + l_{Cu-Mg}^{-2}\right)^{1/4} + K_A^0$$
$$= C_2 GM^{1/2}b^{1/2}\left(A_1 \cdot \rho_d + A_2 \cdot N_{Cu-Mg}^{2/3}\right)^{1/4} + K_A^0, \qquad [17]$$

where C_2 is a constant equal to approximately 0.25,[69] K_A^0 is the contribution due to the generation of dislocations unrelated to forest dislocations and solute clusters, and A_1 and A_2 are scaling constants. Figure 9(a) shows a comparison between the predicted K_A (using the calibrated parameter values of $K_A^0 = 20$ MPa and $A_2 = 0.05$) and experimental K_A values (measured from Figure 7 at a plastic strain of 0.02). The predictions are in good agreement with the experimental results, which indicate that Eqs. [16] and [17] are capable of describing the work hardening behaviors of the present NA Al-Cu-Mg alloy. By defining the percent of the solute cluster contribution to work hardening as $\Omega = A_2 \cdot N_{Cu-Mg}^{2/3}/\left(A_1 \cdot \rho_d + A_2 \cdot N_{Cu-Mg}^{2/3}\right)$, the dependence of Ω on PS is shown in Figure 9(b). It is revealed that, although solute clusters greatly contribute to yield
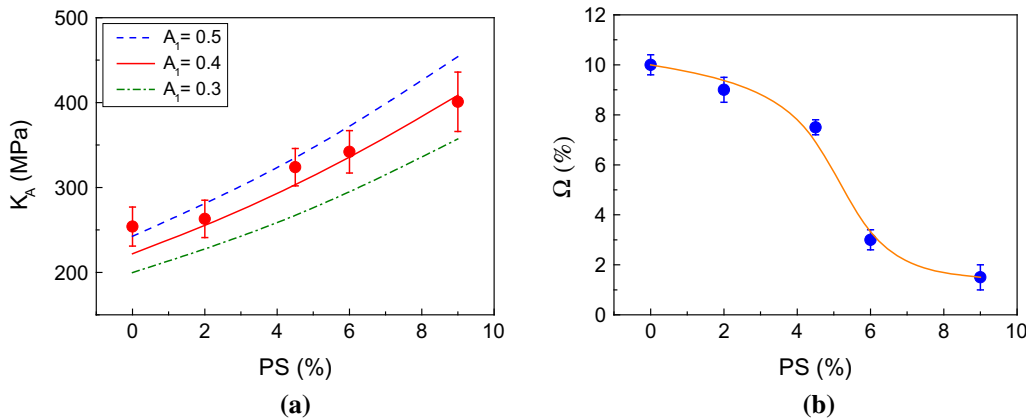

Fig. 9—Plots of K_A (a) and Ω (b) vs PS. The curves in (a) are calculated results from Eq. [17]. Ω represents the percentage of solute-cluster contribution to work hardening, i.e., $\Omega = A_2 \cdot N_{Cu-Mg}^{2/3}/\left(A_1 \cdot \rho_d + A_2 \cdot N_{Cu-Mg}^{2/3}\right)$, with $A_1 = 0.4$.

strength, they only play a minor role in work hardening. This occurs because the shearable clusters are ineffective in increasing the dislocation storage.

V. CONCLUSIONS

1. Dislocations introduced by application of pre-strain to an Al-Cu-Mg alloy accelerate the formation of solute clusters at the initial stage of natural aging while suppressing the formation of new clusters during prolonged aging. This is responsible for a decrease in the final number density of solute clusters after long-term aging and a reduction in cluster strengthening with increasing pre-strain.

2. Variations of electrical resistivity and hardness with the logarithm of the natural aging time exhibit two regimes in the alloy under different pre-strains in the range of 0 to 9.0 pct. In regime I, with an aging time of less than approximately 27 hours, a linear relationship is evident. While in regime II, with an aging time longer than 27 hours, both the electrical resistivity and hardness show no significant changes. The slopes of the lines within regime I are highly dependent on the pre-strain, which is quantitatively described by the development of an *ad hoc* model that considers the effect of pre-existing dislocations.

3. The contributions of solute clusters to yield strength and work hardening were quantitatively estimated and modeled. Solute cluster strengthening in a naturally aged alloy is comparable to dislocation strengthening. Work hardening, however, is predominantly controlled by pre-existing dislocations and is less affected by the solute clusters.

REFERENCES

1. M. Ferrante and R.D. Doherty: *Acta Metall.*, 1979, vol. 27, pp. 1603–14.
2. K.R. Kinsman, H.I. Aaronson, and C. Laird: *Acta Metall.*, 1967, vol. 15, pp. 1244–48.
3. A. Deschamps, G. Fribourg, Y. Bréchet, J.L. Chemin, and C.R. Hutchinson: *Acta Mater.*, 2012, vol. 60, pp. 1905–16.
4. S.P. Ringer and K. Hono: *Mater. Charact.*, 2000, vol. 44, pp. 101–31.
5. A. Biswas, D.J. Siegel, C. Wolverton, and D.N. Seidman: *Acta Mater.*, 2011, vol. 59, pp. 6187–6204.
6. R.K.W. Marceau, G. Sha, R. Ferragut, A. Dupasquier, and S.P. Ringer: *Acta Mater.*, 2010, vol. 58, pp. 4923–39.
7. R.K.W. Marceau, A. de Vaucorbeil, G. Sha, S.P. Ringer, and W.J. Poole: *Acta Mater.*, 2013, vol. 61, pp. 7285–7303.
8. A. Serizawa, S. Hirosawa, and T. Sato: *Metall. Mater. Trans. A*, 2008, vol. 39A, pp. 243–51.
9. G. Sha, R.K.W. Marceau, X. Gao, B. Muddle, and S.P. Ringer: *Acta Mater.*, 2011, vol. 59, pp. 1659–70.
10. E. Clouet, L. Lae, T. Epicier, W. Lefebvre, M. Nastar, and A. Deschamps: *Nat. Mater.*, 2006, vol. 5, pp. 482–88.
11. Z.Q. Zheng, W.Q. Liu, Z.Q. Liao, S.P. Ringer, and G. Sha: *Acta Mater.*, 2013, vol. 61, pp. 3724–34.
12. Y. Chen, N. Gao, G. Sha, S.P. Ringer, and M.J. Starink: *Mater. Sci. Eng. A*, 2015, vol. 627, pp. 10–20.
13. A. Deschamps, T.J. Bastow, F. de Geuser, A.J. Hill, and C.R. Hutchinson: *Acta Mater.*, 2011, vol. 59, pp. 2918–27.
14. C.R. Hutchinson, P.T. Loo, T.J. Bastow, A.J. Hill, and J. da Costa: Teixeira*Acta Mater.*, 2009, vol. 57, pp. 5645–53.
15. T.J. Bastow and S. Celotto: *Acta Mater.*, 2003, vol. 51, pp. 4621–30.
16. M.D.H. Lay, H.S. Zurob, C.R. Hutchinson, T.J. Bastow, and A.J. Hill: *Metall. Mater. Trans. A*, 2012, vol. 43A, pp. 4507–13.
17. B. Klobes, T.E.M. Staab, M. Haaks, K. Maier, and I. Wieler: *Phys. Status Solidi R*, 2008, vol. 2, pp. 224–26.
18. J. Banhart, M.D.H. Lay, C.S.T. Chang, and A.J. Hill: *Phys. Rev. B*, 2011, vol. 83, p. 014101.
19. S. Pogatscher, E. Kozeschnik, H. Antrekowitsch, M. Werinos, S.S.A. Gerstl, J.F. Löffler, and P.J. Uggowitzer: *Scr. Mater.*, 2014, vol. 89, pp. 53–56.
20. M.J. Starink, N. Gao, and J.L. Yan: *Mater. Sci. Eng. A*, 2004, vols. 387–389, pp. 222–26.
21. B. Klobes, K. Maier, and T.E.M. Staab: *Mater. Sci. Eng. A*, 2011, vol. 528, pp. 3253–60.
22. S. Pogatscher, H. Antrekowitsch, H. Leitner, T. Ebner, and P. Uggowitzer: *Acta Mater.*, 2011, vol. 59, pp. 3352–63.
23. S. Esmaeili, X. Wang, D.J. Lloyd, and W.J. Poole: *Metall. Mater. Trans. A*, 2003, vol. 34A, pp. 751–63.
24. H.S. Zurob and H. Seyedrezai: *Scr. Mater.*, 2009, vol. 61, pp. 141–44.
25. Q.L. Zhao: *Scr. Mater.*, 2014, vols. 84–85, pp. 43–46.
26. M.J. Starink and S.C. Wang: *Acta Mater.*, 2009, vol. 57, pp. 2376–89.
27. L. Girifalco and H. Herman: *Acta Metall.*, 1965, vol. 13, pp. 583–90.
28. S Hirosawa, T Sato, J Yokota, and A Kamio: *Mater. Trans., JIM*, 1998, vol. 39, pp. 139–46.
29. R. Nagai, S. Tanigawa, and M. Doyama: *Scr. Metall.*, 1976, vol. 10, pp. 529–31.
30. A. Somoza, A. Dupasquier, I.J. Polmear, P. Folegati, and R. Ferragut: *Phys. Rev. B*, 2000, vol. 61, pp. 14464–69.
31. S. Esmaeili, D. Vaumousse, M.W. Zandbergen, W.J. Poole, A. Cerezo, and D.J. Lloyd: *Philos. Mag.*, 2007, vol. 87, pp. 3797–816.
32. V. Fallah, J. Stolle, N. Ofori-Opoku, S. Esmaeili, and N. Provatas: *Phys. Rev. B*, 2012, vol. 86, p. 134112.
33. V. Fallah, N. Ofori-Opoku, J. Stolle, N. Provatas, and S. Esmaeili: *Acta Mater.*, 2013, vol. 61, pp. 3653–66.
34. F. De Geuser, B.M. Gable, and B.C. Muddle: *Philos. Mag.*, 2010, vol. 91, pp. 315–36.
35. S.P. Ringer, T. Sakurai, and I. Polmear: *Acta Mater.*, 1997, vol. 45, pp. 3731–44.
36. S.P. Ringer, K. Hono, T. Sakurai, and I.J. Polmear: *Scr. Mater.*, 1997, vol. 36, pp. 517–21.
37. A. de Vaucorbeil, C.W. Sinclair, and W.J. Poole: *Philos. Mag.*, 2013, vol. 93, pp. 3664–79.
38. M.J. Starink, L.F. Cao, and P.A. Rometsch: *Acta Mater.*, 2012, vol. 60, pp. 4194–4207.
39. G. Albertini, E. Girardin, A. Giulianli, D.E. Ilie, B.P. O'Donnell, J.P. McGarry, and P.E. McHugh: *Adv. Comp. Lett.*, 2005, vol. 14, pp. 123–29.

40. G. Liu, J. Sun, C.W. Nan, and K.H. Chen: *Acta Mater.*, 2005, vol. 53, pp. 3459–68.
41. G. Liu, G.J. Zhang, R.H. Wang, W. Hu, J. Sun, and K.H. Chen: *Acta Mater.*, 2007, vol. 55, pp. 273–84.
42. G. Liu, G.J. Zhang, X.D. Ding, J. Sun, and K.H. Chen: *Mater. Sci. Eng. A*, 2003, vol. 344, pp. 113–24.
43. B.A. Chen, G. Liu, R.H. Wang, J.Y. Zhang, L. Jiang, J.J. Song, and J. Sun: *Acta Mater.*, 2013, vol. 61, pp. 1676–90.
44. R. Gu and A.H.W. Ngan: *Acta Mater.*, 2012, vol. 60, pp. 6102–11.
45. G.K. Williamson and R.E. Smallman: *Philos. Mag.*, 1956, vol. 1, pp. 34–46.
46. J. Gubicza, I. Schiller, N.Q. Chinh, J. Illy, Z. Horita, and T.G. Langdon: *Mater. Sci. Eng. A*, 2007, vols. 460–461, pp. 77–85.
47. L. Jiang, J.K. Li, P.M. Cheng, G. Liu, R.H. Wang, B.A. Chen, J.Y. Zhang, J. Sun, M.X. Yang, and G. Yang: *Sci Rep.*, 2014, vol. 4, p. 3605.
48. D. Vaumousse, A. Cerezo, and P.J. Warren: *Ultramicroscopy*, 2003, vol. 95, pp. 215–21.
49. I. Kovaćs, J. Lendvai, and E. Nagy: *Acta Metall.*, 1972, vol. 20, pp. 975–83.
50. W. Desorbo, H.N. Treaftis, and D. Turnbull: *Acta Metall.*, 1958, vol. 6, pp. 401–13.
51. Y. Aruga, M. Kozuka, Y. Takaki, and T. Sato: *Mater. Sci. Eng. A*, 2015, vol. 631, pp. 86–96.
52. R. Ferragut, A. Somoza, and I. Torriani: *Mater. Sci. Eng. A*, 2002, vol. 334, pp. 1–5.
53. A. Serizawa, T. Sato, and M.K. Miller: *Mater. Sci. Eng. A*, 2013, vol. 561, pp. 492–97.
54. F.D. Fischer, J. Svoboda, F. Appel, and E. Kozeschnik: *Acta Mater.*, 2011, vol. 59, pp. 3463–72.
55. P. Zhang, S.X. Li, and Z.F. Zhang: *Mater. Sci. Eng. A*, 2011, vol. 529, pp. 62–73.
56. E. Sachs: Z. Ver. Deutsch. Ing, 1928, pp. 734–36.
57. GI. Taylor: J. Inst. Metals, 1938, vol. 62, pp. 307–24.
58. G. Tempus, W. Calles, and G. Scharf: *Mater. Sci. Technol.*, 1991, vol. 7, pp. 937–45.
59. M.J. Starink and S.C. Wang: *Acta Mater.*, 2003, vol. 51, pp. 5131–50.
60. S.P. Yuan, G. Liu, R.H. Wang, X. Pu, G.J. Zhang, J. Sun, and K.H. Chen: *Scr. Mater.*, 2007, vol. 57, pp. 865–68.
61. H. Hargarter, M.T. Lyttle, and E.A. Starke: *Mater. Sci. Eng. A*, 1998, vol. 257, pp. 87–99.
62. N. Hansen: *Scr. Mater.*, 2004, vol. 51, pp. 801–06.
63. M.J. Starink, X. Cheng, and S. Yang: *Acta Mater.*, 2013, vol. 61, pp. 183–92.
64. A. de Vaucorbeil, W.J. Poole, and C.W. Sinclair: *Mater. Sci. Eng. A*, 2013, vol. 582, pp. 147–54.
65. U.F. Kocks and H. Mecking: *Prog. Mater. Sci/*, 2003, vol. 48, pp. 171–273.
66. J. da Costa Teixeira, L. Bourgeois, C.W. Sinclair, and C.R. Hutchinson: *Acta Mater/*, 2009, vol. 57, pp. 6075–89.
67. G. Fribourg, Y. Bréchet, A. Deschamps, and A. Simar: *Acta Mater.*, 2011, vol. 59, pp. 3621–35.
68. Y. Estrin and H. Mecking: *Acta Metall.*, 1984, vol. 32, pp. 57–70.
69. M.F. Ashby, in A. Kelly, R. Nicholson: Elsevier Pub Co, 1971, pp. 137.
70. M.J. Starink, X.G. Qiao, J. Zhang, and N. Gao: *Acta Mater.*, 2009, vol. 57, pp. 5796–5811.